Nanoscale Chemical Imaging of Coadsorbed Thiolate Self-assembled Monolayers on Au(111) by Tip-Enhanced Raman Spectroscopy

Originally published in:
Analytical Chemistry 94(3), https://doi.org/10.1021/acs.analchem.1c03968

Funding acknowledgement:
741431 - Nanoscale Vibrational Spectroscopy of Sensitive 2D Molecular Materials (EC)

Supporting Information

Nanoscale Chemical imaging of Coadsorbed Thiolate Self-assembled Monolayers on Au(111) by Tip-enhanced Raman Spectroscopy

Feng Shao,[1,2] * Liqing Zheng,[2] Jinggang Lan,[3] Renato Zenobi[2*]

[1] *Department of Physics and Astronomy, National Graphene Institute, University of Manchester, Manchester, M13 9PL, UK*

[2]*Department of Chemistry and Applied Biosciences, ETH Zurich, CH-8093, Zurich, Switzerland*

[3]*Department of Chemistry, University of Zurich, Zurich 8057, Switzerland*

**Corresponding Authors: feng.shao@manchester.ac.uk; zenobi@org.chem.ethz.ch*

Table of Contents

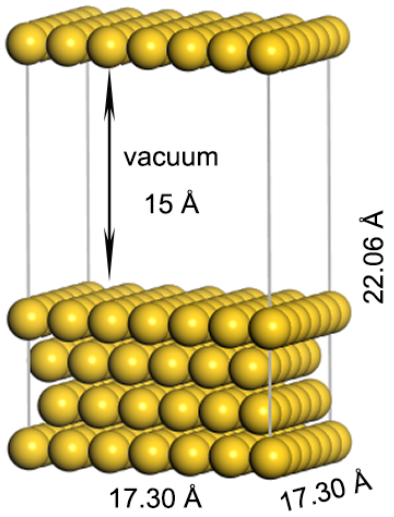

Figure S1. The periodic model (17.03 Å × 17.03 Å × 22.06 Å) used to simulate Au(111) surfaces by a four-layer slab with 36 (6 × 6) atoms in each layer. The slabs were separated by a vacuum space of 15 Å to avoid the interaction between the molecules and the adjacent slab surface. Periodic boundary conditions were applied in all directions of space.

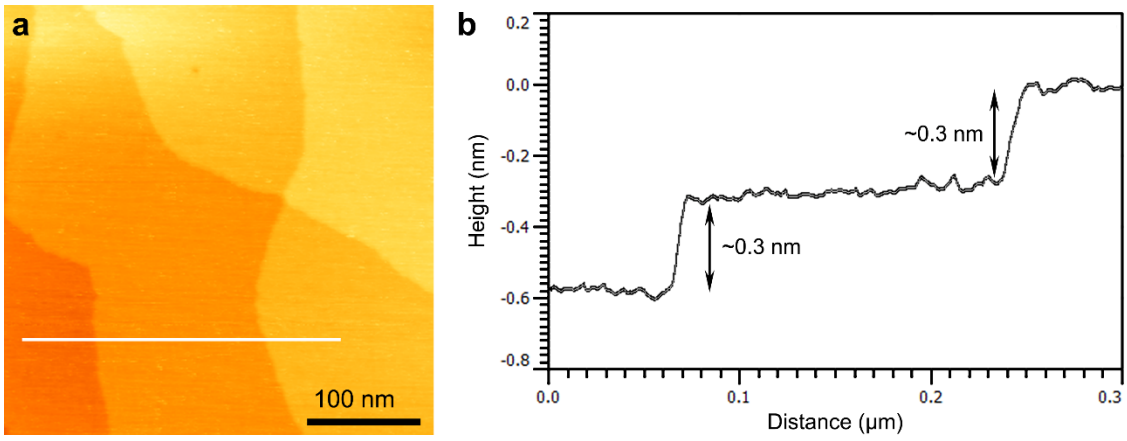

Figure S2. (a) STM image of a bare Au(111) surface using a mechanically cut Pt-Ir tip. (b) Corresponding profile of the scan indicated by the white line in (a). Atomically flat areas and single-atom steps were observed. The bias voltage was 0.1V, and the tunneling current was 1.0 nA.

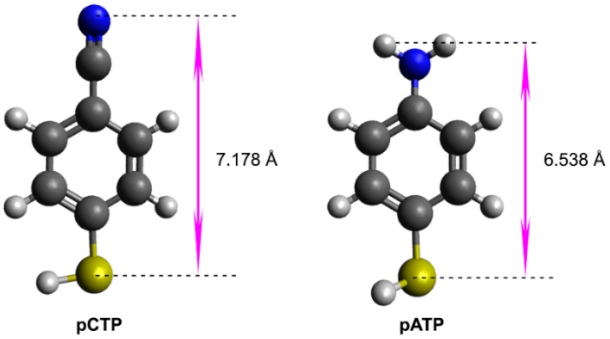

Figure S3. Optimized molecular structure and height of pCTP and pATP in vacuum.

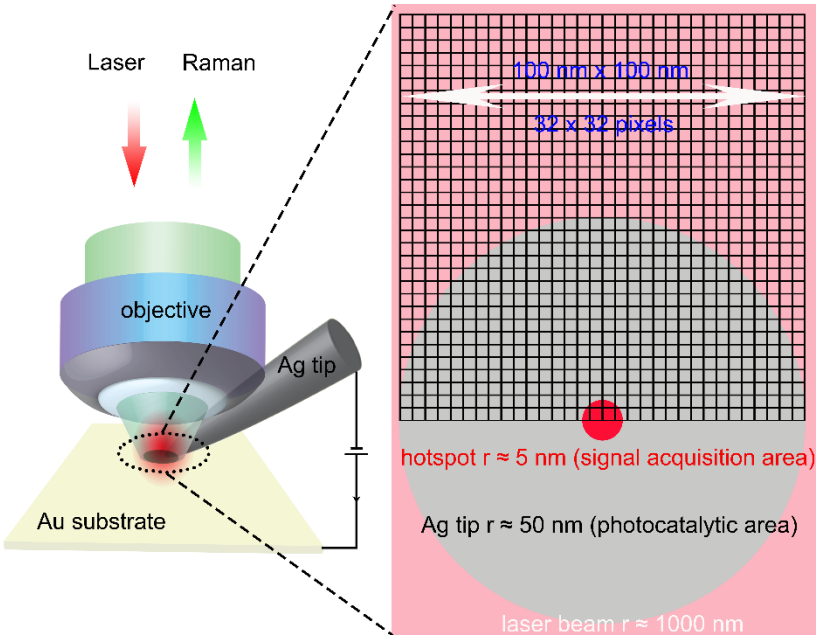

Figure S4. Schematic illustration of the TERS setup and corresponding dimensions of the working areas. The top-illumination configuration allows for exciting and collecting the Raman spectra along the same optical pathway. The incident laser illuminates the sample surface perpendicularly along the tip apex from the top. The curvature radius (r) of the laser beam focus (pink area, r ≈ 1000 nm), Ag tip (gray circle, r ≈ 50 nm), and hotspot (red circle, r ≈ 5 nm) have been discussed in our previous work.[1] Note that more photocatalytic reactions (e.g., pATP to DMAB) could be triggered simultaneously in the gray area during TERS imaging because this area is close to the Ag tip/Au substrate nano-gap and under laser irradiation. Additionally, since all the TERS maps (100 nm × 100 nm, 32 × 32 pixels) are recorded from bottom to top, the upper half part of the TERS image allows for the photocatalytic conversion even longer. This, accordingly, leads to the fact that we can observe stronger DMAB signals (1440 cm^{-1}) and peak ratios (I_{1440} to I_{1586}) at the latter/upper half of the map (Figure 2e).

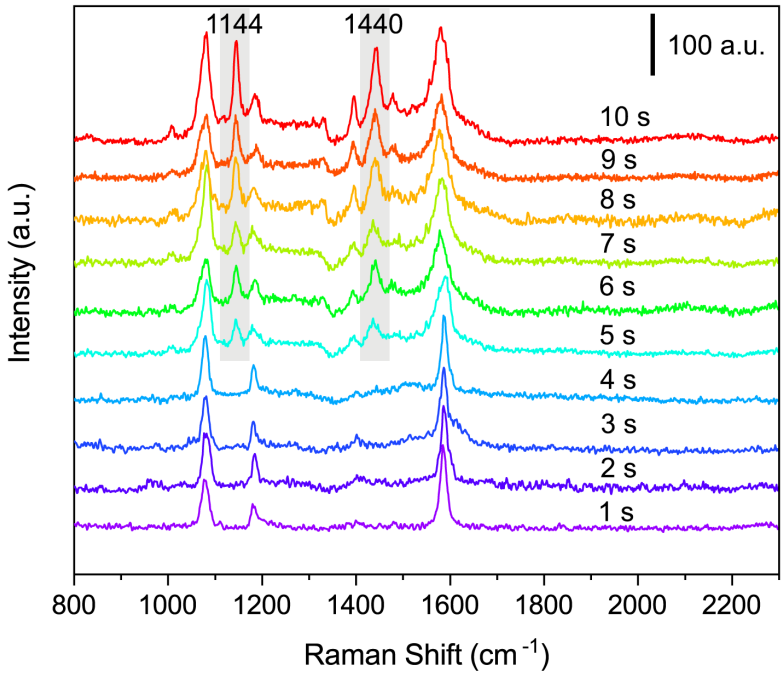

Figure S5. Time-dependent TER spectral evolution of pATP and DMAB in the STM-TERS nanogap (0.1 V, 1.0 nA) under laser excitation (633 nm, 0.5 mW). Serial TER spectra were acquired with an integration time of 1 s. All measurements were carried out by positioning the Ag tip on a fixed location within the pATP/Au(111) SAMs. The characteristic bands of DMAB at 1144 and 1440 cm^{-1} are highlighted in gray areas. The peak ratios (I_{1440} to I_{1586}) of the spectra recorded at 4 s and 5 s are estimated to be around 0.17 and 0.43, respectively. Based on the quality of these two spectra, we suggest that the peak ratio (I_{1440} to I_{1586}) between these two values (ca. 0.3) could indicate the formation of DMAB.

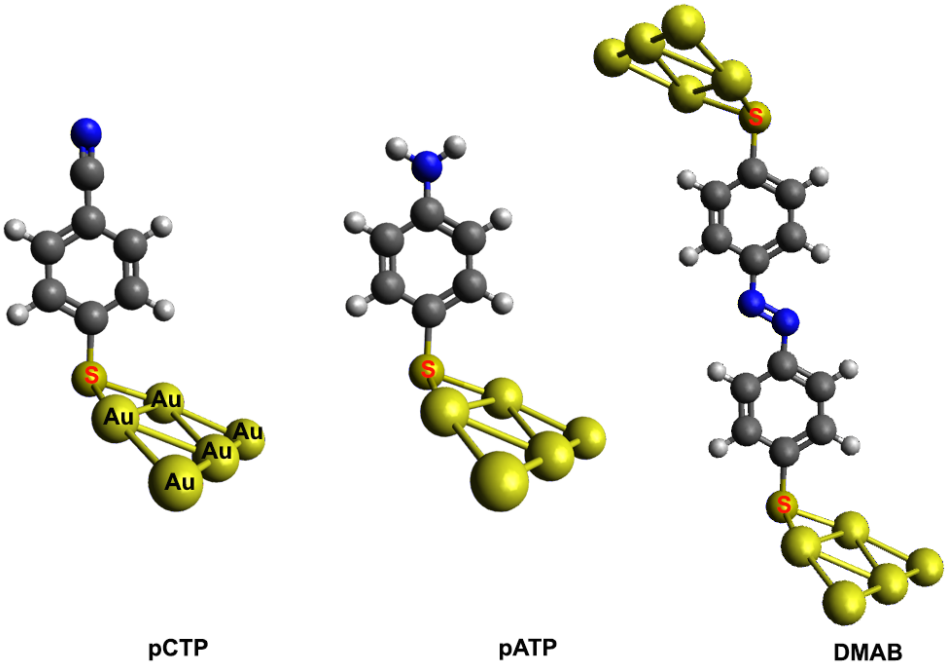

Figure S6. Optimized Au-thiolate geometries using B3LYP/6-311+G** level and LANL2DZ basis set in vacuum.[2] To simplify the calculations, metallic cluster models were used to extract the adsorption structures and simulated spectra of pCTP, pATP, and DMAB on Au(111), based on previous methods proposed by Wu *et al*.[2-5] The selected Au_5 metal clusters allow the thiol S atom to bind to bridge sites, which is the 'standard model' for monothiolates binding on Au(111).[6] Note that the relative intensities of simulated spectra are different from corresponding TERS results (Table S1), which is probably due to a lack of consideration of charge transfer effects and surface selection rules in the DFT calculations.[3-5, 7]

Table S1. Theoretical frequencies and assignments of selected fundamental vibrational bands of pCTP, pATP, and DMAB.[8, 9]

TERS frequencies (cm^{-1})	DFT frequencies (cm^{-1})	Assignments
pCTP		
1080	1068	ν(C-S) + α(ring breathing)
1182	1180	in-plane δ(C-H)
1586	1596	in-plane α(ring) + in-plane δ(C-H)
2230	2285	ν(C≡N)
pATP		
1082	1072	ν(C-S) + α(ring breathing)
1180	1181	in-plane δ(C-H)
1587	1603	in-plane α(ring) + in-plane δ(C-H) + ω(H-N-H)
DMAB		
1082	1064	ν(C-S) + α(ring breathing)
1144	1136	ν(C-N) + in-plane δ(C-H)
1183	1190	in-plane δ(C-H) + ν(C-N)
1395	1460	ν(N=N) + in-plane δ(C-H) + in-plane α(ring)
1440	1498	ν(N=N) + in-plane δ(C-H) + in-plane α(ring)
1590	1598	in-plane α(ring) + ν(N=N) + in-plane δ(C-H)

Abbreviation: ν, stretching; α, in-plane ring deformation; δ, in-plane bending; ω, wagging.

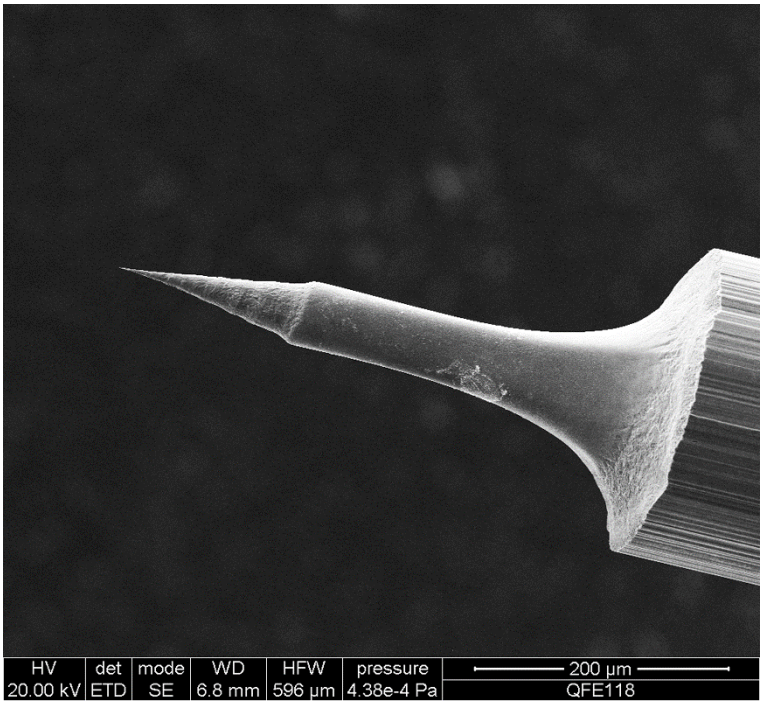

Figure S7. SEM image of a typical Ag tip used for STM-TERS imaging.

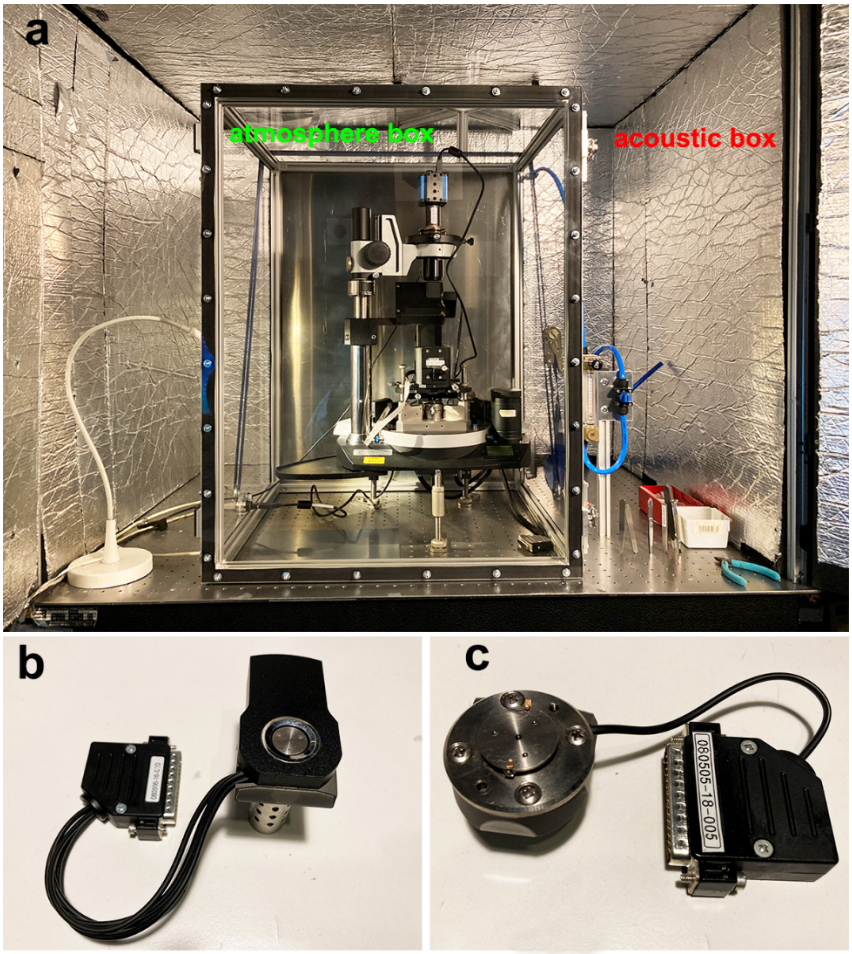

Figure S8. (a) Photo of the upgraded TERS system with the acoustic/atmosphere box. This acoustic isolation box is helpful to reduce ambient noise. (b) Photo of the old piezo scanner (~ 100 μm × 100 μm). (c) Photo of the new piezo scanner (~ 6.0 μm × 6.0 μm). The smaller scanner ensures highly precise control of the tip–substrate gap and *xy* coordinate with a < 0.1 nm step size.

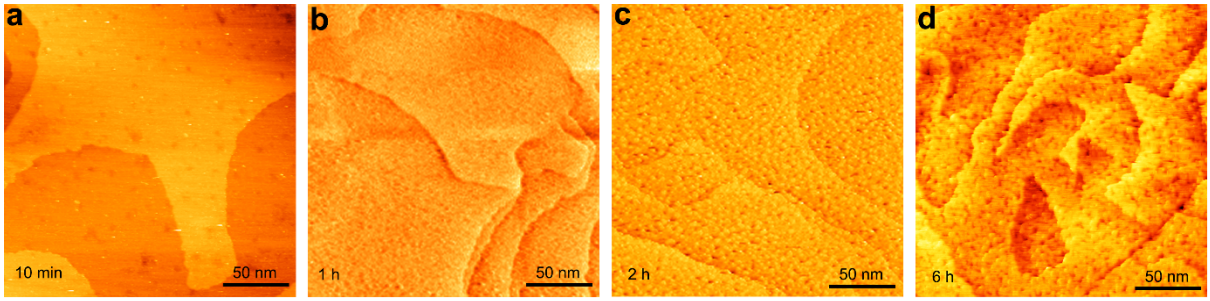

Figure S9. Ex-situ high-resolution STM images of pCTP/pATP binary SAMs on Au(111) with different coadsorption time using mechanically cut Pt-Ir tips: (a) 10 min; (b) 1 h; (c) 2 h; (d) 6 h.

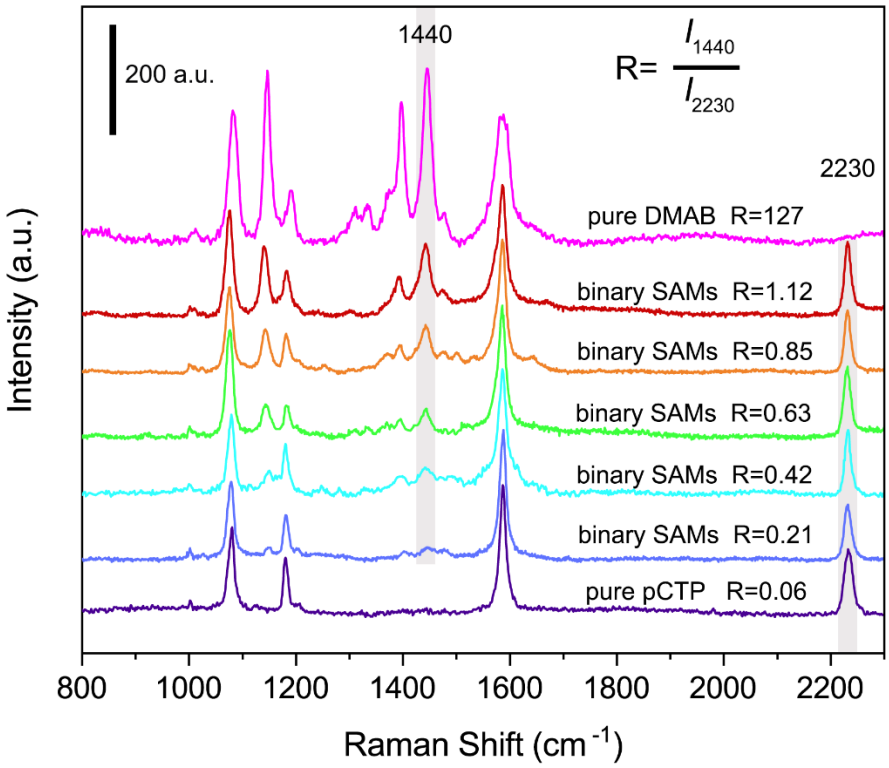

Figure S10. Typical TER spectra of pure and binary pCTP/DMAB adsorbed on Au(111) with different peak intensity ratios (R, I_{1440} to I_{2230}). The color coding of these spectra is in line with their pixel colors in Figure 3. Since the C≡N stretching mode at 2230 cm^{-1} for pCTP was visible in all the binary SAMs at all times, it was used as a standard peak to produce the intensity ratio maps, and the peak intensity ratio was used to indicate the presence of DMAB in the binary SAMs. Compared to pure pCTP (R=0.06) and DMAB (R=127) SAMs, the intensity ratios of typical binary SAMs lie in the 0.6-0.8 range (Figure 3b). Based on the quality of the spectrum with R=0.21, we suggest that the peak ratio (I_{1440} to I_{2230}) over 0.2 ($R \geqslant 0.2$) could indicate the presence of DMAB within the binary SAMs.

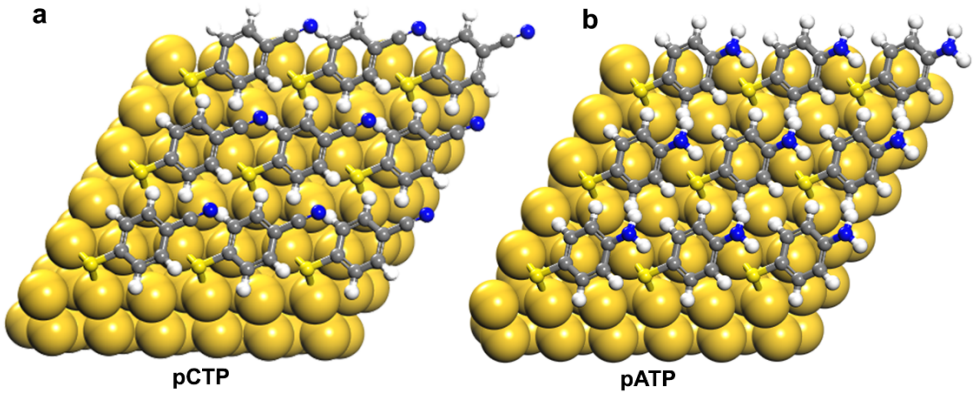

Figure S11. Top view of the optimized configuration of (a) pCTP and (b) pATP adsorbed on Au(111) in vacuum. 3 × 3 thiolate molecules were placed on the 6 × 6 Au(111) surface with coverage of 1/4 monolayer.

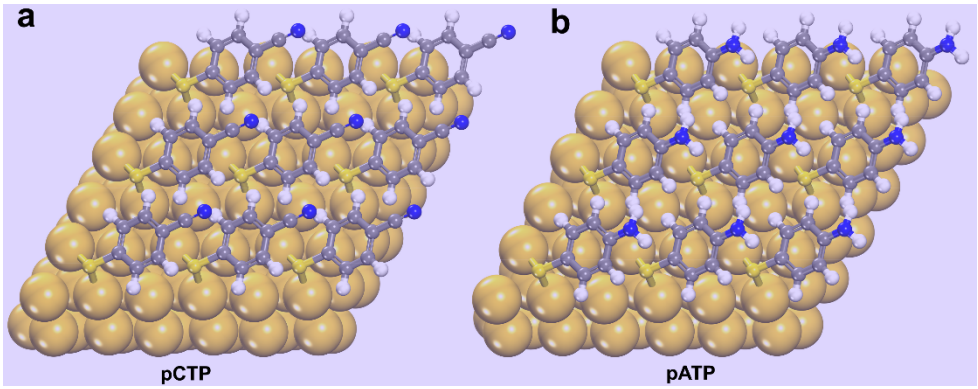

Figure S12. Top view of the optimized configuration of (a) pCTP and (b) pATP adsorbed on Au(111) in methanol. 3 × 3 thiolate molecules were placed on the 6 × 6 Au(111) surface with coverage of 1/4 monolayer.

Table S2. Calculation of the adsorption energy of individual pCTP molecules on Au(111) in vacuum and methanol.

	Adsorption energy of individual pCTP (ΔE_{ads} , eV)	
	-0.62	**-0.92**
Systems	**in vacuum (eV)**	**in methanol (eV)**
Complex	-145570.2259	-145582.3106
Slab	-130305.9122	-130315.2191
pCTP	-1711.212955	-1711.212955
H_2	-31.59022997	-31.59022997

Table S3. Calculation of the adsorption energy of individual pATP molecules on Au(111) in vacuum and methanol.

	Adsorption energy of individual pATP (ΔE_{ads} , eV)	
	-0.82	**-0.84**
Systems	**in vacuum (eV)**	**in methanol (eV)**
Complex	-144477.9881	-144487.4326
Slab	-130305.9122	-130315.2191
pATP	-1589.64543	-1589.64543
H_2	-31.59022997	-31.59022997

REFERENCES

(1) Shao, F.; Wang, W.; Yang, W.; Yang, Z.; Zhang, Y.; Lan, J.; Dieter Schlüter, A.; Zenobi, R., In-situ nanospectroscopic imaging of plasmon-induced two-dimensional [4+4]-cycloaddition polymerization on Au(111). *Nat. Commun.* **2021,** *12* (1), 4557.

(2) Wang, X.; Zhong, J.-H.; Zhang, M.; Liu, Z.; Wu, D.-Y.; Ren, B., Revealing Intermolecular Interaction and Surface Restructuring of an Aromatic Thiol Assembling on Au(111) by Tip-Enhanced Raman Spectroscopy. *Anal. Chem.* **2016,** *88* (1), 915-921.

(3) Huang, Y.-F.; Wu, D.-Y.; Zhu, H.-P.; Zhao, L.-B.; Liu, G.-K.; Ren, B.; Tian, Z.-Q., Surface-enhanced Raman spectroscopic study of p-aminothiophenol. *Phys. Chem. Chem. Phys.* **2012,** *14* (24), 8485-8497.

(4) Wu, D.-Y.; Zhao, L.-B.; Liu, X.-M.; Huang, R.; Huang, Y.-F.; Ren, B.; Tian, Z.-Q., Photon-driven charge transfer and photocatalysis of p-aminothiophenol in metal nanogaps: a DFT study of SERS. *Chem. Commun.* **2011,** *47* (9), 2520-2522.

(5) Wu, D.-Y.; Liu, X.-M.; Huang, Y.-F.; Ren, B.; Xu, X.; Tian, Z.-Q., Surface Catalytic Coupling Reaction of p-Mercaptoaniline Linking to Silver Nanostructures Responsible for Abnormal SERS Enhancement: A DFT Study. *J. Phys. Chem. C* **2009,** *113* (42), 18212-18222.

(6) Häkkinen, H., The gold–sulfur interface at the nanoscale. *Nat. Chem.* **2012,** *4* (6), 443-455.

(7) Shao, F.; Zenobi, R., Tip-enhanced Raman spectroscopy: principles, practice, and applications to nanospectroscopic imaging of 2D materials. *Anal. Bioanal. Chem.* **2019,** *411* (1), 37-61.

(8) Sun, J.-J.; Su, H.-S.; Yue, H.-L.; Huang, S.-C.; Huang, T.-X.; Hu, S.; Sartin, M. M.; Cheng, J.; Ren, B. Role of Adsorption Orientation in Surface Plasmon-Driven Coupling Reactions Studied by Tip-Enhanced Raman Spectroscopy. *J. Phys. Chem. Lett.* **2019,** *10* (10), 2306-2312.

(9) Wang, C.-F.; Cheng, Z.; O'Callahan, B. T.; Crampton, K. T.; Jones, M. R.; El-Khoury, P. Z. Tip-Enhanced Multipolar Raman Scattering. *J. Phys. Chem. Lett.* **2020,** *11* (7), 2464-2469.